

Masquerading hybrid stars with dark matter

Carline Biesdorf,^{1,*} Jürgen Schaffner-Bielich,² and Laura Tolos^{3,4,5}

¹*Departamento de Física, CFM - Universidade Federal de Santa Catarina; C.P. 476, CEP 88.040-900, Florianópolis, SC, Brasil*

²*Institut für Theoretische Physik, J. W. Goethe Universität,*

Max von Laue-Str. 1, 60438 Frankfurt am Main, Germany

³*Institute of Space Sciences (ICE, CSIC), Campus UAB,*

Carrer de Can Magrans, 08193, Barcelona, Spain

⁴*Institut d'Estudis Espacials de Catalunya (IEEC), 08860 Castelldefels (Barcelona), Spain*

⁵*Frankfurt Institute for Advanced Studies, Ruth-Moufang-Str. 1, 60438, Frankfurt am Main, Germany*

Abstract: We investigate the influence of dark matter on hybrid stars. Using a two-fluid approach, where normal and dark matter components interact only gravitationally, we explore how dark matter can trigger the appearance of quark matter in neutron stars for unprecedented low masses. Our findings reveal that dark matter increases the central pressure of neutron stars, potentially leading to the formation of hybrid stars with quark cores even at very low compact star masses. The critical mass for the appearance of quark matter decreases with increasing dark matter content. We introduce the concept of "masquerading hybrid stars", where dark matter admixed stars exhibit similar mass-radius relations to purely hadronic stars, making it challenging to distinguish between them based solely on these parameters. Additionally, we identify a unique class of objects termed "dark oysters", characterized by a large dark matter halo and a small normal matter core, highlighting the diverse structural possibilities for compact stars influenced by dark matter.

Keywords: dark matter, hybrid stars, two-fluid approach, dark oysters

I. INTRODUCTION

Astrophysical and cosmological observations indicate that most of the mass of the Universe appears in the form of non-baryonic mass/energy [1–3]. Whereas the Universe is composed of only 4.9% of baryonic matter, an invisible form of matter called dark matter (DM), whose existence is inferred from its gravitational effects, rises up to 26.4% [4]. Another component, dark energy (DE), whose existence is related to the accelerated expansion of the Universe, generates 68.7% of its total mass.

The nature of DM is, however, still puzzling. A lot of candidates have been proposed, with masses ranging from 10^{-33} GeV (Fuzzy DM) to 10^{15} GeV (Wimpzillas). Whereas there are direct methods for detecting DM using particle accelerators [5, 6] or analyzing DM scattering off nuclear targets in terrestrial detectors [7], no evidence of its existence has been produced so far. An alternative for testing the possible effects of DM are the compact objects (COs), such as white dwarfs (WDs) and neutron stars (NSs). Because of their extreme densities, the probability of the interaction of DM with normal (or ordinary) matter (NM) could be large and the DM capture would be increased [8–10].

The authors of [8, 11–16] have investigated the gravitational collapse of NSs caused by DM accretion in various indirect searches for DM, aiming to establish constraints on its properties. Additionally, [17] examines the accretion of DM in Sun-like and supermassive stars, followed by their collapse into either NSs or WDs. There have also been investigations into how the presence of DM

affects the cooling patterns of compact stars, which will ultimately undergo self-annihilation [10, 18–23]. Furthermore, studies have focused on the alterations in the kinematic properties of NSs resulting from the accretion of self-annihilating DM [24].

Based on the idea that the current DM abundance has a similar origin as visible matter, an appealing alternative to WIMPs is the asymmetric dark matter (ADM) model. WIMPs are supersymmetric particles, based on the assumption of a symmetry between bosons and fermions. If, on the other hand, nature is parity symmetric, we have a different form of DM, mirror matter [25]. Because ADM is non-annihilating it can accumulate, producing changes in mass and radius of the stars, possibly forming extraordinary compact NSs. Comparing the mass-radius relation predicted by star models with NM and with NM admixed with DM in NSs, it is possible to extract information on DM and the equation of state (EoS) of the NSs. Several studies in this regard have been already performed [21, 25–72] including studies of excitation modes in the presence of DM [73, 74]. However, only a very few of these kind of analysis have been performed on hybrid stars. To the best of our knowledge, only refs. [57] and [75] have performed such studies.

Once the quantum chromodynamics (QCD) phase diagram with its possible phase transitions became a research field of high interest, the possibility that NSs could, in fact, contain both a hadronic and a quark phase, started to be explored [76–78]. Asymptotic freedom enables matter to become deconfined when density increases even at low temperatures. Thus, as the density augments toward the star's core, quarks may become more energetically favorable than baryons, leading to the possibility that the core of a NS could be made up of deconfined quarks. If the entire star does not convert itself

* carline.fsc@gmail.com

into a quark star, as suggested by the Bodmer-Witten conjecture [79, 80], the final composition is a quark core surrounded by an hadronic layer. This is what is generally called a hybrid star [81, 82]. We note that in modern terms the QCD phase transition of interest at high densities is the chiral phase transition with the chiral condensate being the order parameter not the deconfinement phase transition. However, of interest for us is that there is the possibility of a first order phase transition at high densities to be studied below.

Given that DM may compress even further what is already an incredible dense object, it is interesting to analyze how the existence of DM could influence the presence of quark matter (QM) in the interior of NSs. In the present paper we investigate this possible scenario. To that end we consider an EoS for a hybrid star built via Maxwell construction from a Quantum Hadrodynamics (QHD)-based model, for nucleons and hyperons, and a MIT-based model, for u-d-s quarks matter, as already done in [83]. For the DM EoS we use a non-self annihilating self-interacting Fermi gas with different interaction strengths and two different particle masses, $m_D = 5$ GeV and $m_D = 100$ GeV [84]. These two fluids, NM and DM, only interact gravitationally. Compared to Refs. [57] and [75], even though we use the same model for NM, in these previous works the authors only considered one fluid made of NM interacting with DM through the exchange of a Higgs boson in the former and through the exchange of a scalar as well as a vector meson in the latter. So, to the best of our knowledge, the present work is the first to analyze the effect of DM on hybrid stars using a two-fluid approach.

The present paper is organized as follows. In Section II we present the coupled Tolman-Oppenheimer-Volkov (TOV) equations used to obtain the mass-radius diagrams for a two-fluid system and in Section III we show the EoSs for these two fluids. In Section IV we describe the stability analysis performed in the present work, which follows the recent procedure described in [53], that considers the changes in stability that NM might induce on DM, and vice versa. The analysis of the results starts in Sec. V with Subsection V A, where we show that, in fact, the addition of DM can trigger the early appearance of QM, thus leading to hybrid stars much earlier than expected due to the presence of DM, an effect we refer to as masquerading hybrid stars with DM. In Section V B we discuss the size of the QM core in this hybrid configurations with DM and how it relates with the different interaction strengths and particle mass of the DM. And, finally, in Section V C we take a closer look to the strongly interacting DM case for a small DM particle mass, demonstrating that compact stars with a small NM core containing QM can be produced with very large DM radii.

II. STELLAR STRUCTURE EQUATIONS

In the following we describe the basic equations of our investigations of DM admixed hybrid stars, where DM is a non-self annihilating self-interacting Fermi gas and hybrid matter is made of NM formed by nucleons, hyperons and QM. These two fluids only interact gravitationally and, hence, in order to compute the macroscopic properties of DM admixed hybrid stars, we solve the TOV equations, which, in their dimensionless form are given [84]:

$$\begin{aligned} \frac{dp'_{NM}}{dr} &= -(p'_{NM} + \epsilon'_{NM}) \frac{d\nu}{dr}, \\ \frac{dm_{NM}}{dr} &= 4\pi r^2 \epsilon'_{NM}, \\ \frac{dp'_{DM}}{dr} &= -(p'_{DM} + \epsilon'_{DM}) \frac{d\nu}{dr}, \\ \frac{dm_D}{dr} &= 4\pi r^2 \epsilon'_{DM}, \\ \frac{d\nu}{dr} &= \frac{(m_{NM} + m_D) + 4\pi r^3 (p'_{NM} + p'_{DM})}{r(r - 2(m_{NM} + m_D))}, \end{aligned} \quad (1)$$

where $p' = P/m_D^4$ and $\epsilon' = \epsilon/m_D^4$ are the dimensionless pressure and energy density, respectively, being m_D the DM particle mass¹. The physical mass and radius of each species are given by $R_i = (M_p/m_D^2)r_i$ and $M_i = (M_p^3/m_D^2)m_i$, respectively, where $i = \{NM, DM\}$ and M_p is the Planck mass [84].

As will become clear later on, in order to analyze the stability of the mass-radius configurations, we also need to compute the total number of particles of each species. And for that we solve the following equation for the two number conservations together with the TOV equations above:

$$\frac{dN'_i}{dr} = 4\pi \frac{n'_i}{\sqrt{1 - 2(m_{NM} + m_D)/r}} r^2 \quad (2)$$

where $n'_i = n_i/m_D^3$ and N'_i are the dimensionless number density and the total number, respectively, of $i = \{NM, DM\}$. We obtain the number of particles for each species by re-scaling them as $N_i = N'_i \cdot M_p^3/m_f^3$ (see Ref. [84]).

III. MICROSCOPIC MODELS

A. DM Equation of State

For DM the EoS is taken from [84] for a non-self annihilating self-interacting Fermi gas. The dimensionless

¹ In order to obtain the dimensionless quantities for each fluid we could also divide the physical quantities by a NM particle, as the neutron mass. However, it is important to divide all physical quantities by the same mass scale.

energy density, pressure and number density are given by, respectively:

$$\epsilon'_{DM} = \frac{1}{8\pi^2} \left[(2z^3 + z)(1 + z^2)^{1/2} - \sinh^{-1}(z) \right] \quad (3)$$

$$+ \left(\frac{1}{3\pi^2} \right)^2 y^2 z^6,$$

$$p'_{DM} = \frac{1}{24\pi^2} \left[(2z^3 - 3z)(1 + z^2)^{1/2} + 3\sinh^{-1}(z) \right] \quad (4)$$

$$+ \left(\frac{1}{3\pi^2} \right)^2 y^2 z^6$$

$$n'_{DM} = \frac{n_{DM}}{m_D^3} = \frac{z^3}{3\pi^2},$$

where z is the dimensionless Fermi momentum and $y = m_D/m_I$ the interaction strength, with m_I being the energy scale of the interaction between fermions. Note that for $y \ll 1$ the EoS will be the one of an ideal Fermi gas.

Here we will explore the cases of y varying from weakly interacting ($y = 10^{-1}$) to strongly interacting ($y = 10^3$) DM. As for the mass of the DM particle, we will also explore two cases: $m_D = 5$ GeV and $m_D = 100$ GeV. In Fig. 1 we show four representative dimensionful DM EoSs for the two DM particle masses and for the two different interaction strength parameters discussed here.

B. NM Equations of State

For the NM we construct a hybrid EoS using the Maxwell construction as criteria to define the hadron-quark phase transition.

To describe hadronic matter we use the Walecka Model [85] with non-linear terms [86], ω - ρ meson coupling terms and inclusion of the ϕ meson that only couples to the hyperons. The EoS can be derived from the following Lagrangian density:

$$\begin{aligned} \mathcal{L}_{NLWM} = & \sum_B \bar{\psi}_B [\gamma_\mu (i\partial^\mu - g_{B\omega}\omega^\mu - g_{B\rho}\frac{\vec{\tau}_B}{2}\vec{\rho}^\mu - g_{B\phi}\phi^\mu) - m_B^*] \psi_B + \frac{1}{2}\partial_\mu\sigma\partial^\mu\sigma - \frac{1}{2}m_\sigma^2\sigma^2 - \frac{1}{3!}\kappa\sigma^3 - \frac{1}{4!}\lambda\sigma^4 \\ & - \frac{1}{4}\Omega^{\mu\nu}\Omega_{\mu\nu} + \frac{1}{2}m_\omega^2\omega_\mu\omega^\mu - \frac{1}{4}\vec{R}_{\mu\nu}\vec{R}^{\mu\nu} + \frac{1}{2}m_\rho^2\vec{\rho}_\mu\vec{\rho}^\mu + \Lambda_v g_{N\omega}^2 g_{N\rho}^2 \omega_\mu\omega^\mu \vec{\rho}_\mu\vec{\rho}^\mu - \frac{1}{4}\Phi^{\mu\nu}\Phi_{\mu\nu} + \frac{1}{2}m_\phi^2\phi_\mu\phi^\mu, \quad (5) \end{aligned}$$

where the Dirac spinor ψ_B represents the baryons with the effective mass $m_B^* = m_B - g_{B\sigma}\sigma$, $\vec{\tau}_B$ are the corresponding Pauli matrices, g_{Bi} are the coupling constants of the mesons $i = \sigma, \omega, \rho, \phi$ with the baryon B , m_i is the mass of the meson i , $\Omega_{\mu\nu} = \partial_\mu\omega_\nu - \partial_\nu\omega_\mu$, $\vec{R}_{\mu\nu} = \partial_\mu\vec{\rho}_\nu - \partial_\nu\vec{\rho}_\mu - g_\rho(\vec{\rho}_\mu \times \vec{\rho}_\nu)$ and $\Phi_{\mu\nu} = \partial_\mu\phi_\nu - \partial_\nu\phi_\mu$. The quantities κ and λ are scalar self-interaction constants responsible for softening the EoS of symmetric nuclear matter around saturation density, while allowing to obtain a realistic value for the compression modulus of nuclear matter, introduced in [86, 87]. The Λ_v is the coupling constant of the mixed quartic isovector-vector interaction that modifies the density dependence of the nuclear symmetry energy [88, 89]. The B sum extends over the octet of the lightest baryons $\{n, p, \Lambda, \Sigma^-, \Sigma^0, \Sigma^+, \Xi^-, \Xi^0\}$.

are

$$\sigma_0 = \sum_B \frac{g_{B\sigma} n_B^s}{m_\sigma^2} - \frac{\kappa}{2} \frac{\sigma_0^2}{m_\sigma^2} - \frac{\lambda}{6} \frac{\sigma_0^3}{m_\sigma^2}, \quad (6)$$

$$\omega_0 = \sum_B \frac{g_{B\omega} n_B}{m_\omega^2} - \frac{\xi}{6} \frac{g_\omega^4 \omega_0^3}{m_\omega^2} - \frac{2\Lambda_v g_\omega^2 g_\rho^2 \bar{\rho}_{0(3)}^2 \omega_0}{m_\omega^2}, \quad (7)$$

$$\bar{\rho}_{0(3)} = \sum_B \frac{g_{B\rho} I_3 n_B}{m_\rho^2} - \frac{2\Lambda_v g_\omega^2 g_\rho^2 \omega_0^2 \bar{\rho}_{0(3)}}{m_\rho^2}, \quad (8)$$

$$\phi_0 = \sum_B \frac{g_{B\phi} n_B}{m_\phi^2}, \quad (9)$$

where n_B^s and n_B are the scalar and baryon densities for each baryon species, with the total scalar n_S and baryon (hadron) n_H densities given by

$$n_S = \sum_B \frac{1}{\pi^2} \int dk_B \cdot k_B^2 \frac{m_B^*}{\sqrt{k_B^2 + m_B^{*2}}}, \quad (10)$$

$$n_H = \sum_B \frac{1}{\pi^2} \int dk_B \cdot k_B^2. \quad (11)$$

After applying the mean-field approximation, the EoS can be easily obtained from Eq. (5). The mesonic fields

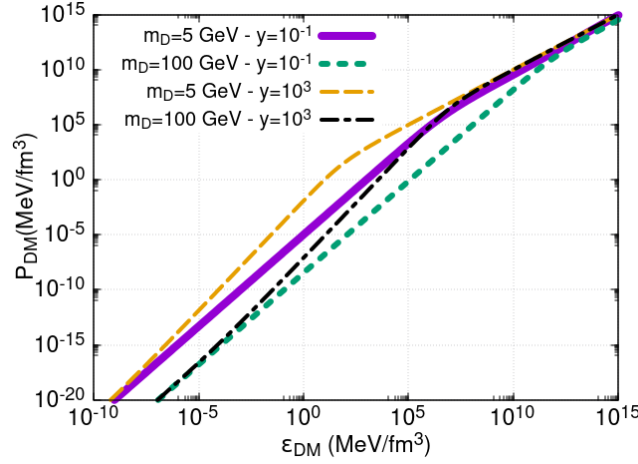


FIG. 1. DM EoSs for weakly ($y = 10^{-1}$) and strongly ($y = 10^3$) interacting matter and for the two DM particle masses ($m_D = 5$ GeV and $m_D = 100$ GeV) considered in this work.

The energy density and pressure then read

$$\begin{aligned} \epsilon_H = & \sum_B \frac{1}{\pi^2} \int dk_B \cdot k_B^2 \sqrt{k_B^2 + m_B^{*2}} \\ & + \frac{1}{2} (m_\sigma^2 \sigma_0^2 + m_\omega^2 \omega_0^2 + m_\rho^2 \rho_{0(3)}^2 + m_\phi^2 \phi_0^2) \\ & + \frac{\kappa}{3!} \sigma_0^3 + \frac{\lambda}{4!} \sigma_0^4 + \frac{\xi}{8} g_\omega^4 \omega_0^4 + 3\Lambda_v g_\omega^2 g_\rho^2 \omega_0^2 \rho_{0(3)}^2, \end{aligned} \quad (12)$$

$$\begin{aligned} P_H = & \sum_B \frac{1}{3\pi^2} \int dk_B \cdot \frac{k_B^4}{\sqrt{k_B^2 + m_B^{*2}}} \\ & - \frac{1}{2} (m_\sigma^2 \sigma_0^2 - m_\omega^2 \omega_0^2 - m_\rho^2 \rho_{0(3)}^2 - m_\phi^2 \phi_0^2) \\ & - \frac{\kappa}{3!} \sigma_0^3 - \frac{\lambda}{4!} \sigma_0^4 + \frac{\xi}{4!} g_\omega^4 \omega_0^4 + \Lambda_v g_\omega^2 g_\rho^2 \omega_0^2 \rho_{0(3)}^2. \end{aligned} \quad (13)$$

We choose the NL3* $\omega\rho$ model, which is the NL3* parametrization proposed in [90] with the addition of the $\omega\rho$ -channel as done in [91]. This parametrization has the following nuclear saturation parameters: $n_0 = 0.150 \text{ fm}^{-3}$, $E/A = 16.3 \text{ MeV}$, $K = 258 \text{ MeV}$, $E_{sym} = 30.7 \text{ MeV}$, $L = 42 \text{ MeV}$ and $M^*/M = 0.59$, which satisfy the phenomenological constraints taken

from [92, 93]. This parametrization also reproduces maximum star masses above $2 M_\odot$, even when hyperons are included. The main parameters are presented in Table I.

As for hyperons, we consider the hyperon masses to be $m_\Lambda = 1116 \text{ MeV}$, $m_\Sigma = 1193 \text{ MeV}$ and $m_\Xi = 1318 \text{ MeV}$. The couplings of the hyperons to the vector mesons are related to the nucleon couplings, $g_{N\omega}$ and $g_{N\rho}$, by assuming SU(6)-flavour symmetry, according to the ratios [95–100]:

$$\begin{aligned} g_{\Lambda\omega} : g_{\Sigma\omega} : g_{\Xi\omega} : g_{N\omega} &= \frac{2}{3} : \frac{2}{3} : \frac{1}{3} : 1, \\ g_{\Lambda\rho} : g_{\Sigma\rho} : g_{\Xi\rho} : g_{N\rho} &= 0 : 2 : 1 : 1, \end{aligned} \quad (14)$$

$$g_{\Lambda\phi} : g_{\Sigma\phi} : g_{\Xi\phi} : g_{N\phi} = -\frac{\sqrt{2}}{3} : -\frac{\sqrt{2}}{3} : -\frac{2\sqrt{2}}{3} : 1,$$

noting that $g_{N\phi} = 0$. The coupling of each hyperon to the σ field is adjusted to reproduce the hyperon potential in symmetric nuclear matter (SNM) derived from hypernuclear observables. We fix this potentials as $U_\Lambda(n_0) = -28 \text{ MeV}$, $U_\Sigma(n_0) = +30 \text{ MeV}$ and $U_\Xi(n_0) = -4 \text{ MeV}$ and obtain the coupling constants presented in Table II.

To describe the quark matter we use the modified MIT Bag model, as introduced in [101], with the inclusion of a vector field and a self-interacting vector field. The Lagrangian density is as following:

$$\mathcal{L}_{MIT} = \sum_q \left\{ \bar{\psi}_q \left[\gamma^\mu (i\partial_\mu - g_{qqV} V_\mu) - m_q \right] \psi_q + \frac{1}{2} m_V^2 V_\mu V^\mu + b_4 \frac{(g_{uuV}^2 V_\mu V^\mu)^2}{4} - B \right\} \Theta(\bar{\psi}_q \psi_q) - \frac{1}{2} \bar{\psi}_q \psi_q \delta_S, \quad (15)$$

where the Dirac spinor ψ_q represents the quark with mass m_q running over u, d and s , whose values are 4 MeV, 4 MeV and 95 MeV, respectively [102], g_{qqV} the coupling

constant, and m_V the mass of the meson. The quantity $\Theta(\bar{\psi}_q \psi_q)$ is a Heaviside function that ensures that the quarks are confined inside the bag and δ_S is a Dirac

TABLE I. Parameters of the model NL3 $^*\omega\rho$ utilized in this work. The parametrization is taken from Ref. [94]. The meson masses m_σ , m_ω and m_ρ as well as κ are given in MeV. The nucleon and ϕ masses are fixed at $M = 939$ MeV and $m_\sigma = 1020$ MeV, respectively.

m_σ	m_ω	m_ρ	$g_{N\sigma}$	$g_{N\omega}$	$g_{N\rho}$	$\kappa/g_{N\sigma}^3$	$\lambda/g_{N\sigma}^4$	Λ_v
502.574	782.600	763.000	10.0944	12.8065	14.4410	4.1473	-0.017422	0.045

TABLE II. Hyperon- σ coupling constants adjusted to reproduce the hyperon potential in SNM derived from hypernuclear observables.

Model	$g_{\Lambda\sigma}/g_{N\sigma}$	$g_{\Sigma\sigma}/g_{N\sigma}$	$g_{\Xi\sigma}/g_{N\sigma}$
NL3 $^*\omega\rho$	0.613	0.461	0.279

function that guarantees continuity of the fields of the quarks on the surface of the bag. Using the mean-field approximation and solving the Euler-Lagrange equations of motion, we obtain the energy eigenvalues for the quarks and for the V field as follows:

$$E_q = \mu = \sqrt{m_q^2 + k^2} + g_{qqV}V_0, \quad (16)$$

$$\begin{aligned} & g_{uuV}V_0 + \left(\frac{g_{uuV}}{m_v}\right)^2 b_4(g_{uuV}V_0)^3 \\ & = \left(\frac{g_{uuV}}{m_v}\right) \sum_{q=u,d,s} \left(\frac{g_{qqV}}{m_v}\right) n_q. \end{aligned} \quad (17)$$

The baryon density in the quark phase, energy density and pressure are given by

$$n_Q = \sum_q \frac{n_q}{3} = \sum_q \frac{1}{\pi^2} \int dk_q \cdot k_q^2, \quad (18)$$

$$\begin{aligned} \epsilon_Q &= \sum_q \left(\frac{3}{\pi^2} \int dk_q \cdot k_q^2 \sqrt{m_q^2 + k_q^2} \right) + \frac{1}{2} m_V^2 V_0^2 + \\ &+ \frac{3}{4} b_4 (g_{uuV} V_0)^4 + B, \end{aligned} \quad (19)$$

$$\begin{aligned} P_Q &= \sum_q \left(\frac{1}{\pi^2} \int dk_q \frac{k_q^4}{\sqrt{m_q^2 + k_q^2}} \right) + \frac{1}{2} m_V^2 V_0^2 + \\ &+ \frac{1}{4} b_4 (g_{uuV} V_0)^4 - B. \end{aligned} \quad (20)$$

Here we choose the parametrization $B^{1/4} = 155$ MeV, for the Bag pressure value, $G_V = (g_{uuV}/m_V)^2 = 1.0$ fm 2 and $b_4 = 1.2$. As for the relation between the coupling constants we opt to use the ones obtained via symmetry relations, where one has $g_{ssV} = \frac{2}{5}g_{uuV} = \frac{2}{5}g_{ddV}$. This parametrization describes unstable strange matter, which allows the existence of a quark core that will not convert the whole star into a strange star [83].

Neutron stars are charged neutral objects in β -equilibrium. Therefore, in order to produce β -stable matter with zero net charge, we also add leptons as a free Fermi gas to both hadron and quark matter and impose the conditions of β -equilibrium and charge neu-

trality. For hadron matter,

$$\begin{aligned} \mu_B = \mu_n - q_B \mu_e \quad \text{and} \quad \mu_e = \mu_\mu, \\ n_p + n_{\Sigma^+} = n_{e^-} + n_{\mu^-} + n_{\Sigma^-} + n_{\Xi^-}, \end{aligned} \quad (21)$$

whereas for quark matter

$$\begin{aligned} \mu_s = \mu_d = \mu_u + \mu_e \quad \text{and} \quad \mu_e = \mu_\mu, \\ n_{e^-} + n_{\mu^-} = \frac{1}{3}(2n_u - n_d - n_s). \end{aligned} \quad (22)$$

As for the inner and outer crust of the stars, we use [103] and [104], respectively and for $\epsilon < 3.3 \times 10^3$ g/cm 3 we use the Harrison-Wheeler EoS [105].

We also impose an upper limit on the NM EoS and allow pressures only up to 1000 MeV/fm 3 , which corresponds to a density around $12n_0$, where n_0 is the nuclear saturation density. So we stay far below the density at which the EOS from perturbative QCD (pQCD) is known, which is about $40n_s$ [106].

Note that the EoSs for the hadron and quark phases are dimensionful. Therefore, in order to solve Eqs. (1) together with Eq. (2), we will scale the pressure and energy density with the DM particle mass, as done for the DM EoS.

1. The Hybrid EoS

Once the EoSs for the hadron and quark phases are known, we can build the EoS to describe hybrid stars, i.e., compact stars with a core of QM surrounded by hadron matter. For that purpose we use the Maxwell construction. In this case the necessary conditions for thermodynamic equilibrium of the hadronic and quark phases allowing a first order phase transition are given by:

$$\mu_0^H = \mu_0^Q \quad \text{and} \quad P_0^H = P_0^Q, \quad (23)$$

where μ_0 for the hadrons and quarks are

$$\begin{aligned} \mu_0^H &= \frac{(\sum_B \mu_B n_B + \sum_l \mu_l^H n_l^H)}{\sum_B n_B}, \\ \mu_0^Q &= \frac{3(\sum_q \mu_q n_q + \sum_l \mu_l^Q n_l^Q)}{\sum_q n_q}. \end{aligned} \quad (24)$$

There is no experimental evidence about the value of the baryon chemical potential at the hadron-quark interface, μ_0 , at zero temperature. An inferior limit of 1050 MeV

P_0 (MeV/fm ³)	μ_0 (MeV)	μ_H (MeV/fm ³)	μ_Q (MeV/fm ³)
361	1698	1003	1280

TABLE III. Main thermodynamic values at the hadron-quark phase transition. These quantities will remain the same throughout the entire paper.

was pointed out in [107] using the Polyakov loop formalism. In [83] an upper limit of $\mu_0 = 1400$ MeV was adopted based on the discussion of Ref. [78], where the authors also point out that QM inside massive neutron stars is not only possible but probable. Here, however, we relax this condition and use a higher value for μ_0 , as can be seen in Table III. As the first hyperons start to appear around $n_H = 0.31$ fm⁻³, at a chemical potential of $\mu_H = 1135$ MeV, which is below the value of μ_0 , this choice of parametrizations also justifies the inclusion of these more massive baryons, besides the nucleons. The quantities shown in table III for the phase transition point will remain the same throughout this entire work and will play an important role determining at which mass of the NS the hadron-quark phase transition will occur.

In order to construct the EoS to describe hybrid stars, one needs to ensure that uds-quark matter is unstable ($E=A > 930$ MeV). Otherwise, as soon as the core of the star converts to the quark phase, the entire star may convert into a quark star in a finite amount of time [108]. As already mentioned above, the parametrization chosen here ensures that uds-quark matter is unstable. However, this specific choice of parameters for the MIT model in combination with the QHD model has an even more profound meaning. If used to describe single-uid stars, the hadron-quark phase transition happens only when NSs become unstable, i.e., with this combination of parametrizations, all the dynamically stable stars ($M = M_{\text{max}} > 0$) are purely hadronic. The reason for this choice is to emphasise the effect of the DM on the hadron-quark phase transition, as will become clear later on. Furthermore, the choice for the QHD parametrization ensures that we still meet the constraints imposed by PSR J070+6620 [109] and PSR J0952-0607 [110]. In Fig. 2 we show the hybrid EoS (top) and the corresponding mass-radius diagram (bottom) obtained by solving the single-uid TOV equations.

IV. STABILITY ANALYSIS

In order to draw conclusions on the effect of DM on hybrid stars we have to first check where our mass-radius configurations are dynamically stable. In the case of a single uid, the stability analysis is based on considering small perturbations from the hydrostatic equilibrium and then solve a Sturm-Liouville problem, which results in n eigenfrequencies ω_n that obey the discrete hierarchy $\omega_n^2 < \omega_{n+1}^2$, $n = 0; 1; 2; \dots$, with $\omega_0^2 > 0$. If $\omega_0^2 < 0$, then the lowest energy mode is imaginary, indicating an instability. To determine the sign of the mode one can,

FIG. 2. EoS (top) and mass-radius relation (bottom). No stable hybrid star is possible within these parametrizations.

instead of solving the eigenvalue problem, analyze the dependence of the star's total mass and radius as a function of its central energy density (or central pressure). The extrema in the mass versus energy density (or pressure) indicates a change in the sign of eigenfrequency associated to a certain mode. If the derivative of the radius versus the energy density (or pressure) at that energy density is negative (positive) an even (odd) mode is changing sign. So, starting from low energy densities where all modes are positive, it is then possible to perform the stability analysis for higher energy densities studying the change in sign of the eigenfrequency modes and checking when the lowest one becomes negative (see Ref. [111] for more details).

In Refs. [36, 37, 45] the above described stability analysis was applied to a two uid system. In that case this method is used for the two species of matter separately (NM and DM) and the compact object is found stable only when both species of matter are stable. However, this naive stability analysis does not consider the changes in stability that NM might induce on DM and vice versa. Therefore here we will make use of a different method

based on the one developed by [112] and expanded in [33, 113–116]. More precisely, we will follow closely what was done in [53]. This method is based on the fact that at the onset of unstable radial modes, the total number of fluid elements N must be stationary under the variations of the central energy density ϵ_c , i.e., $\partial N/\partial\epsilon_c = 0$. This criteria is consistent with the more commonly used criteria $\partial M/\partial\epsilon_c = 0$ as, under the assumption of uniform entropy per baryon, the stellar mass is stationary under any transformation $\epsilon(r) \rightarrow \epsilon(r) + \delta\epsilon(r)$ that leaves the total number of fluid elements N unchanged [117] and this is true if and only if the TOV equations are satisfied, i.e., only for equilibrium configurations.

In the case of a two-fluid star the TOV Eqs. (1) and (2) are satisfied if and only if any transformation $\epsilon_i(r) \rightarrow \epsilon_i(r) + \delta\epsilon_i(r)$ that leaves $\delta N_i = 0$ also leaves the total mass unchanged $\delta M = 0$, with $i = \{NM, DM\}$.

The condition that N_i are stationary is given by

$$\begin{pmatrix} \delta N_{NM} \\ \delta N_{DM} \end{pmatrix} = \begin{pmatrix} \partial N_{NM}/\partial\epsilon_c^{NM} & \partial N_{NM}/\partial\epsilon_c^{DM} \\ \partial N_{DM}/\partial\epsilon_c^{NM} & \partial N_{DM}/\partial\epsilon_c^{DM} \end{pmatrix} \begin{pmatrix} \delta\epsilon_c^{NM} \\ \delta\epsilon_c^{DM} \end{pmatrix} = 0. \quad (25)$$

As the small shifts in the energy density are not zero, $\delta\epsilon_c^i \neq 0$, we have that

$$\frac{\partial N_{NM}}{\partial\epsilon_c^{NM}} \frac{\partial N_{DM}}{\partial\epsilon_c^{DM}} - \frac{\partial N_{NM}}{\partial\epsilon_c^{DM}} \frac{\partial N_{DM}}{\partial\epsilon_c^{NM}} = 0, \quad (26)$$

which is the criteria for the onset of radial instability for two-fluid stars. So we have that, at the onset of instability, $\delta N_i = 0$ and $\delta M = 0$ under variations of the central energy densities, $(\epsilon_c^{NM}, \epsilon_c^{DM}) \rightarrow (\epsilon_c^{NM} + \delta\epsilon_c^{NM}, \epsilon_c^{DM} + \delta\epsilon_c^{DM})$.

For a two-fluid system, the matrix above can be diagonalized and one obtains two independent sets of variables, (ϵ_c^A, N_A) and (ϵ_c^B, N_B) corresponding to eigenvalues κ_A and κ_B . As N_A and N_B are linear combinations of N_{NM} and N_{DM} , they are also conserved and kept fixed when the star is perturbed. So, if small and independent changes to ϵ_c^A and ϵ_c^B are performed, the stable solutions should satisfy:

$$\kappa_A > 0 \quad \text{and} \quad \kappa_B > 0. \quad (27)$$

This generalizes the widely used stability condition $\partial M/\partial\epsilon_c > 0$ to multi-fluid stars [53]. In the present work we will use the condition given by Eq. (27) to determine if our solutions are stable or not.

V. RESULTS

A. Dark Matter Admixed Hybrid Stars

Several works have already analyzed the effect of DM on the whole mass-radius diagram, i.e., on the NS branch as well as on the WD branch. Even though different EoSs have been used to describe NM, the results yield the same

general conclusions, the main one being that, when one of the central pressures significantly exceeds the other, the fluid with the higher central pressure takes over, causing the system to act as if it consists of a single fluid. Also, the pressure at which DM starts to prevail depends on its mass as well as on its interaction strength. For more details the interested reader can refer, for example, to [36, 37, 45, 71]. Here we focus on the NS branch and analyze how the presence of DM could favor the appearance of hybrid stars.

We start by defining a critical mass M_{crit} as the minimum mass of a star that has a quark core, i.e., stars with masses below M_{crit} are purely hadronic or are DM admixed hadronic stars, but without quark matter in its core. At the microscopic level this means that the star with M_{crit} is the one with a central pressure of NM equal to the pressure where the hadron-quark phase transition happens, i.e., $P_0 = 361 \text{ MeV/fm}^3$, so that all the stars with higher NM central pressure are hybrid stars.

In Fig. 3 we show the total mass ($M_T = M_{NM} + m_D$) versus the observable radius (R_{NM}) for different ratios of DM central pressure versus the NM one (P_{DM}/P_{NM}). We display the stable mass-radius configurations with DM with different colored solid lines, whereas in violet solid lines we depict the mass-radius relation without DM for comparison. Note that in the top left plot we can vary P_{DM}/P_{NM} up to 7×10^6 and the mass-radius solutions will still be on top of the mass-radius configurations without DM. We consider weakly interacting DM (left panels) and strongly interacting DM (right panels) as well as two values of DM particle masses ($m_D = 100 \text{ GeV}$ for top plots and $m_D = 5 \text{ GeV}$ for bottom ones). The triangular and hexagonal points in each plot show the location of the M_{crit} for different P_{DM}/P_{NM} ratios. The round black dots indicate the M_{crit} corresponding to the first stable hybrid star to appear, i.e., they correspond to the minimum value of P_{DM}/P_{NM} necessary for the appearance of a stable hybrid star. We remind the reader that, without DM, this branch would correspond to purely hadronic stable stars. However, as can be seen, once we add a certain amount of DM, stable hybrid stars start to appear. We can also observe that the results corresponding to strongly interacting DM with DM particle mass of 5 GeV (right bottom plot) differ substantially from the others. In this last case, we show stable (solid) and unstable (dashed) mass-radius solutions. The black squared dots merely show the location of the M_{crit} for each ratio shown in the plot. For the case without DM and also for $P_{DM}/P_{NM} = 10^3$ the configurations for M_{crit} are unstable.

For $m_D = 100 \text{ GeV}$ as well as $m_D = 5 \text{ GeV}$ with $y = 10^{-1}$, we observe in Fig. 3 that, as P_{DM}/P_{NM} increases, the stable mass-radius configurations are reduced as compared to the case without DM. This is due to the fact that, as already mentioned above, with the increase of P_{DM}/P_{NM} , DM starts to slowly dominate over NM, inducing a change of stability of the configurations. Indeed, the mass-radius solutions migrate to smaller radii

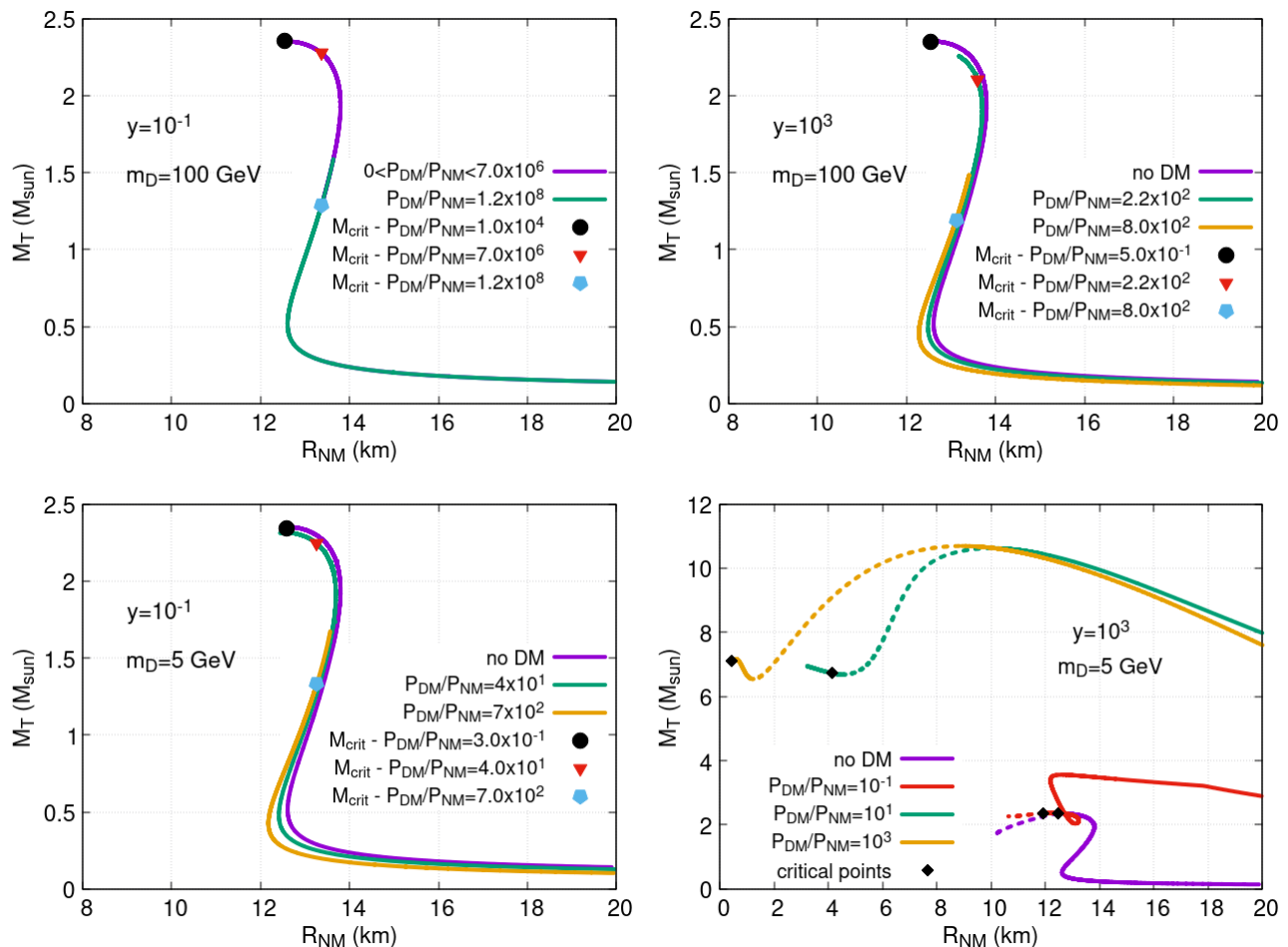


FIG. 3. Total mass ($M_T = M_{NM} + m_D$) as a function of the observable radius (R_{NM} radius) of DM admixed NSs for different pressure ratios (P_{DM}/P_{NM}). We consider weakly $y = 10^{-1}$ (left panels) and strongly $y = 10^3$ (right panels) interacting DM, as well as $m_D = 100$ GeV (top panels) and $m_D = 5$ GeV (bottom panels). The dots indicate the critical mass M_{crit} at which hybrid stars start to appear for each ratio. The round black dots indicate the first hybrid star to appear for each y and m_D . In the bottom right figure we also include unstable results indicated by dashed lines.

and masses as compared to the case without DM, eventually forming dark compact planets (DCPs), with Earth-like or Jupiter-like masses and radii of about one meter or one kilometer, respectively, as shown in Refs. [36, 37]. For the case of $m_D = 5$ GeV and $y = 10^3$ we find, however, a very peculiar behavior, with the total mass growing and the NM radius decreasing (while the DM radius increases) with larger P_{DM}/P_{NM} ratios. In this case we also include the results for smaller radii ($R_{NM} \leq 8$ km). We will analyze these configurations in more details in Sec. V C. Thus, from now on we concentrate on the results for $m_D = 100$ GeV for $y = 10^{-1}$ and $y = 10^3$ as well as $m_D = 5$ GeV for $y = 10^{-1}$.

We can now compare the behavior of the mass-radius configurations among these three cases. We find that for weakly interacting DM one needs to add more DM to obtain the first stable hybrid star than for the strongly interacting case, as can be seen if we compare the results for $m_D = 100$ GeV on the top plots of Fig. 3.

For $y = 10^{-1}$ the first stable hybrid star appears at $P_{DM}/P_{NM} = 1.0 \times 10^4$, whereas for $y = 10^3$ a hybrid star already happens at $P_{DM}/P_{NM} = 5.0 \times 10^{-1}$. Also, for the same interaction strength y , one needs to add more DM when the DM particle mass is larger, as can be seen if we compare the results on the left plots of the same figure for $y = 10^{-1}$. For $m_D = 100$ GeV the first stable hybrid star appears at $P_{DM}/P_{NM} = 1.0 \times 10^4$, whereas for $m_D = 5$ GeV it already appears at $P_{DM}/P_{NM} = 3.0 \times 10^{-1}$.

In order to understand the previously described mass-radius relations, we should address the quantity of DM necessary for the existence of quark matter in a stable hybrid star for different interaction strengths and DM particle masses. For that purpose, we analyze how the NM central pressure evolves with the accumulation of DM (in terms of the P_{DM}/P_{NM} ratio), paying a special attention when the hadron-quark phase transition occurs. In Fig. 4 we display P_{NM} of a $1.4M_\odot$ star as a

function of P_{DM}/P_{NM} for the two DM particle masses cases ($m_D = 5$ GeV and 100 GeV) and different values of the strength interaction $y = 10^{-1}, 10, 10^3$. We also include a line (yellow dotted) representing the pressure at which the hadron-quark phase transition occurs.

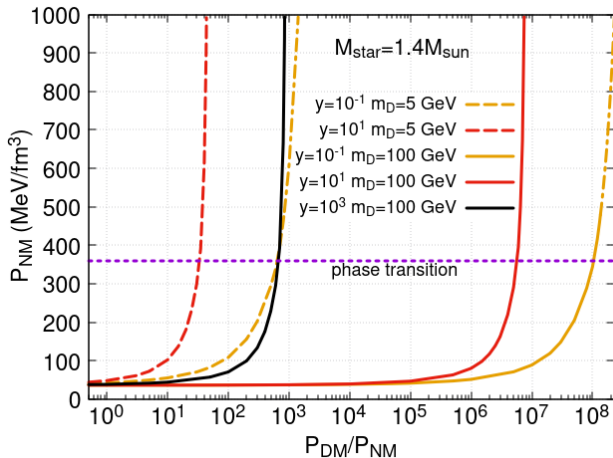


FIG. 4. Central pressure of normal matter (P_{NM}) as a function of the ratio of pressures (P_{DM}/P_{NM}) for a $1.4M_{\odot}$ star, considering $m_D = 5$ GeV (dashed lines) and $m_D = 100$ GeV (solid lines) and different values of the DM interaction strength ($y = 10^{-1}, 10, 10^3$). The yellow dotted line shows the pressure where the hadron-quark phase transition takes place. The dashed-dotted lines indicate unstable configurations.

From Fig. 4 we find that the NM central pressure increases with P_{DM}/P_{NM} . That, ultimately, is what enables us to get stable hybrid stars. As quark matter starts to appear only at pressures equal to $P_{NM} = 361$ MeV/fm³, a star with NM central pressure lower than this value is still completely hadronic, or an hadronic star with DM, but there is no QM in its core. After a certain quantity of DM is added, the central pressure reaches the critical value of 361 MeV/fm³ and the star converts into a hybrid star with a quark core. In the next section, we will discuss the size of this core.

As for the physical meaning of these results, we note the following. When we add DM to NM, the former compresses the latter so that the already dense object gets even more dense so that one needs more NM to get a star with the same mass and approximately the same size. If we go back to Fig. 3, we see that, except for the bottom right plot, we produce a $1.4M_{\odot}$ star for different values of P_{DM}/P_{NM} for each DM particle mass and interaction strength, with similar NM radii. The difference between these $1.4M_{\odot}$ stars is the quantity of DM and, consequently, of NM.

Regarding the change of M_{crit} with the accumulation of DM, in Fig. 5 we plot M_{crit} as a function of P_{DM}/P_{NM} for different values of the DM interaction strength and the two DM masses, as in Fig. 4. We only show results that lead to stable hybrid stars with $8 \leq R_{NM} \leq 20$ km.

As DM compresses NM, the larger the P_{DM}/P_{NM} ratio is, the larger the NM central pressure becomes, allowing, eventually, for the appearance of QM. In other words, without DM a NM central pressure corresponding to the hadron-quark phase transition pressure, i.e., $P_0 = P_C = 361$ MeV/fm³ produces a star of $2.35M_{\odot}$. However, once enough DM is added, the total mass diminishes so that the same NM central pressure now gives rise to a star with less mass. And, the more DM we add, the less mass this NM central pressure can sustain, so M_{crit} decreases until this star becomes unstable or a DCP (both not shown in Fig. 5).

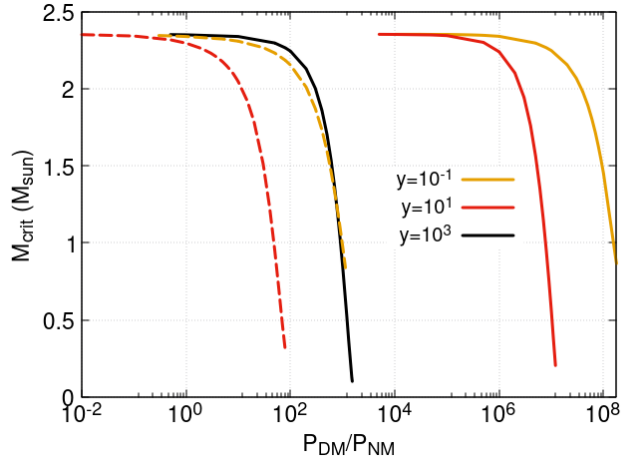


FIG. 5. Critical mass (M_{crit}) as a function of the ratio between pressures (P_{DM}/P_{NM}) for $m_D = 5$ GeV (dashed lines) and $m_D = 100$ GeV (solid lines) and for different values of the interaction strength of the DM (y). Only results associated to stable stars are shown.

In Refs. [57, 75] it was also found that the critical mass decreases with the increase of DM. In these works, as the DM interacts with the NM via Higgs boson or scalar and vector meson exchange, DM makes the EoS softer, which, in turn, leads to a decrease in the maximum mass and the radii move to smaller values.

To close up this section, we summarize our findings. We find that DM does not substitute NM, but that DM allows for more matter to be compressed inside a star, eventually allowing QM to appear. The mass and radius of a star are no longer defined exclusively by one central pressure, but by two. It is clear from Fig. 4 that various combinations of the two central pressures produces a star with the same mass ($1.4M_{\odot}$ in that case) and that the addition of DM results in an increase of the NM central pressure of the star. From Fig. 3 we see that in most cases even the radius does not change much. Therefore, by only analyzing the mass and the radius of the star, it is impossible to know the NM central pressure and if this central pressure allows the appearance of QM. The presence of DM is then masquerading hybrid stars so that neutron stars without QM in the core and hybrid stars with a sufficient amount of DM have a very similar

m_D (GeV)	y	P_{DM}/P_{NM}	$m_D(M_\odot)$	$R_{DM}(\text{km})$
100	10^{-2}	$1.07 \times 10^8 - 1.35 \times 10^8$	$6.25 \times 10^{-5} - 6.15 \times 10^{-5}$	$7.69 \times 10^{-4} - 7.05 \times 10^{-4}$
100	10^{-1}	$1.06 \times 10^8 - 1.35 \times 10^8$	$6.26 \times 10^{-5} - 6.16 \times 10^{-5}$	$7.72 \times 10^{-4} - 7.04 \times 10^{-4}$
100	10^0	$8.60 \times 10^7 - 1.15 \times 10^8$	$6.92 \times 10^{-5} - 6.86 \times 10^{-5}$	$8.22 \times 10^{-4} - 7.27 \times 10^{-4}$
100	10^1	$5.80 \times 10^6 - 7.40 \times 10^6$	$2.57 \times 10^{-4} - 2.84 \times 10^{-4}$	$2.57 \times 10^{-3} - 2.20 \times 10^{-3}$
100	10^2	$6.90 \times 10^4 - 8.50 \times 10^4$	$2.37 \times 10^{-3} - 2.66 \times 10^{-3}$	$2.28 \times 10^{-2} - 1.97 \times 10^{-2}$
100	10^3	$6.80 \times 10^2 - 8.40 \times 10^2$	$2.34 \times 10^{-2} - 2.64 \times 10^{-2}$	$2.28 \times 10^{-1} - 1.98 \times 10^{-1}$
5	10^{-2}	$7.00 \times 10^2 - 8.40 \times 10^2$	$2.49 \times 10^{-2} - 2.45 \times 10^{-2}$	$3.01 \times 10^{-1} - 2.81 \times 10^{-1}$
5	10^{-1}	$6.50 \times 10^2 - 8.40 \times 10^2$	$2.50 \times 10^{-2} - 2.46 \times 10^{-2}$	$3.09 \times 10^{-1} - 2.81 \times 10^{-1}$
5	10^0	$5.20 \times 10^2 - 7.20 \times 10^2$	$2.76 \times 10^{-2} - 2.73 \times 10^{-2}$	$3.31 \times 10^{-1} - 2.89 \times 10^{-1}$
5	10^1	$3.40 \times 10^1 - 4.30 \times 10^1$	$9.90 \times 10^{-2} - 1.10 \times 10^{-1}$	$1.02 \times 10^{-1} - 8.80 \times 10^{-1}$

TABLE IV. Minimum and maximum pressure ratios (P_{DM}/P_{NM}) that result in stable $1.4M_\odot$ DM admixed hybrid stars and the corresponding total DM masses ($m_D(M_\odot)$) and radii ($R_{DM}(\text{km})$) for different values of the interaction strength y and DM particle mass m_D .

mass-radius relation. Moreover, hybrid star configurations with DM can be present for such low neutron star masses at which neutron stars with ordinary matter only would not be considered to have a QM core.

B. Hadrons, Quarks and Dark Matter in Stars

Now we study the quantity of each type of matter (hadrons, QM and DM) contained in a DM admixed hybrid star. In order to do so we analyze again $1.4M_\odot$ hybrid stars for different P_{DM}/P_{NM} ratios. In Fig. 6 we display the total mass of QM (top panel) and the

corresponding radius (bottom panel) as a function of P_{DM}/P_{NM} for stable $1.4M_\odot$ hybrid stars for $m_D = 5$ GeV and $m_D = 100$ GeV and different interaction strengths. Note that the results for $m_D = 5$ GeV and $y = 10^3$ are left for a separate study in Sec.V C. As can be seen, for each combination of y and m_D , the interval of P_{DM}/P_{NM} in which we obtain a stable $1.4M_\odot$ star that is a hybrid star is very tight. As the total DM masses and the corresponding radii vary even less than the QM ones, we present only the minimum and maximum pressure ratios with the corresponding DM masses and radii in Table IV.

The first conclusion we can extract from Fig. 6 is that, for a given m_D , the larger the DM interaction strength is, the larger the QM masses become. And, for a given DM interaction strength, the smaller the m_D is, the larger the QM masses become. This result can be understood from Fig. 4, where we see that the DM parametrization that is more effective in compressing the star also gives rise to more QM, i.e., the changes in QM follow the ones for DM. In [71, 84] it was shown that the total mass of a DM fermionic star grows as the particle mass decreases ($M \propto m_D^{-2}$) and as the interacting strength increases. And in Fig. 6 we can see the same behavior for the QM core, as QM feels the gravitational potential generated by DM, that varies with the interacting strength and/or DM particle mass.

Moreover we find that for each value of m_D and y the larger the P_{DM}/P_{NM} ratio is, the more QM is produced. This can be easily understood if we look again at Fig. 4, the increase of the P_{DM}/P_{NM} ratio also induces larger NM central pressure, which, of course, results in more QM. As for DM, the quantity of DM does not vary much as the interval for P_{DM}/P_{NM} for which we obtain stable stars is tight, remaining almost constant, as seen in Ta-

ble IV. In fact, from Table IV we observe that the DM contribution to the mass slightly decreases when augmenting the pressure ratio for $10^{-2} \leq y \leq 1$, whereas it increases for higher values of y for both values of m_D . In [84] it is shown for a single DM fermionic star that, when keeping the same central pressure and changing the interacting strength, for small values of y , the maximum mass does not change, while it increases with a power law for strong interactions ($y > 1$). Here the DM central pressure is increased, but for small values of y the DM loses the 'competition' to NM, which then appears in the form of QM. So, for small values of y , when increasing the P_{DM}/P_{NM} , the contribution to the total mass from QM increases and from DM decrease, whereas for $y > 1$ the contributions from both types of matter increase with the pressure.

If we now compare the amount of QM mass with respect to the DM mass, we find that the contribution to the total mass coming from DM is much larger. In spite of this, the maximum contribution to the total mass from DM corresponds to less than 8% of the total mass (for $y = 10$, $m_D = 5$ GeV and $P_{DM}/P_{NM} = 43$), showing that the most important contribution to the total mass

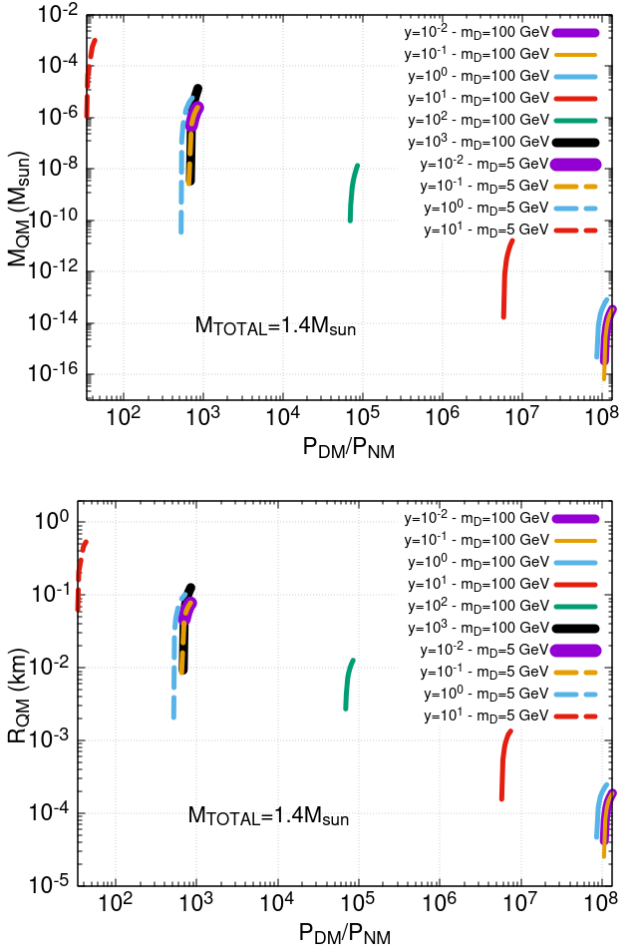


FIG. 6. Mass (top) and radius (bottom) of QM as a function of P_{DM}/P_{NM} in $1.4M_{\odot}$ hybrid stars for different interaction strengths y and masses of the DM particle m_D .

still comes from hadronic matter. For the same values of y , m_D and P_{DM}/P_{NM} we also get the most QM, which is $M_{QM} = 9.85 \times 10^{-4} M_{\odot}$, that corresponds to only 0.07% of the total mass of the star.

With regard to the radii for each type of matter, we obtain that QM accumulates within a small radius at the core of the star, while following the trend of the QM mass, that is, smaller QM masses also mean smaller QM radii, with the radius increasing as the mass augments. The QM radii can be as small as 4.14 cm and reach at most 0.539 km for $y = 10$ and $m_D = 5$ GeV. As for the DM radii, for all the cases shown here, its value is also small but slightly bigger than the QM radii, with values varying from 70.4 cm up to 1.02 km. Note that the DM radius is also quite insensitive to P_{DM}/P_{NM} , slightly decreasing with the ratio, as the increase of the ratio compresses DM. So, in conclusion, most of DM is admixed with QM in the most inner core of $1.4M_{\odot}$, but a small amount of DM is also mixed with hadronic matter.

Up to now we have shown the composition and structure of $1.4M_{\odot}$ DM admixed hybrid stars. However, one

may pose the question of the interplay between QM and DM for larger star masses. Stars with larger masses have higher central pressures without DM. Hence, the ratio P_{DM}/P_{NM} needed to reach the hadron-quark phase transition pressure is smaller and, as a direct consequence, the quantity of DM in those stars will be smaller. However, the amount of QM can be larger. On the other hand, stars with less than $1.4M_{\odot}$ will require more DM as compared to those with larger masses so as to reach the hadron-quark phase transition. Therefore, these low-mass stars will have a bigger and more massive DM core, but a less massive QM core. At the same time, the radius of the DM decreases, so that the DM core of these stars is denser.

Note that in Ref. [57] it was also found that the QM core increases with the increase of DM content. The authors showed that, for example, a QM core of a $2M_{\odot}$ star that already corresponds to approximately 60% of the mass of the star when there is no DM present, can grow up to 80% of the total mass when DM is added.

It is also worth mentioning that we obtain very small QM cores as compared to the ones obtained in other works that explore the possible existence of hybrid stars without DM [83] or in the one-fluid model of interacting NM with DM, as done in Ref. [57]. However, we remind the reader that our present goal is to show that DM can trigger the appearance of QM. Thus, we choose hadronic and QM parametrizations that do not produce stable hybrid stars without DM. With the conclusions drawn here, we can argue that for NM configurations that already allow the appearance of QM, with the addition of DM, the amount of QM can be even larger.

C. Dark Oysters

In this last section, our aim is to analyze the case of strongly interacting DM ($y = 10^3$) with a particle mass of $m_D = 5$ GeV, given the particular mass-radius configurations obtained in Fig. 3.

In the bottom right plot of Fig. 3 we show that the mass-radius configurations are much more sensitive to changes in the P_{DM}/P_{NM} ratio, as compared to the other three cases depicted in the same figure. Also, the mass of the DM admixed stars increases with the pressure ratio. These results stem from the fact that DM dominates over NM as we increase the ratio, so that the total mass is governed by the mass of the DM component, which scales with the inverse of the square of the DM particle mass, as already discussed in [45, 84]. In fact, already at $P_{DM}/P_{NM} = 10^3$, DM completely dominates and a further increase of the ratio will not change much the shape of the $M_T - R_{DM}$ relation, where M_T is the total mass, even though the $M_T - R_{NM}$ relation will still slightly change, as NM will be further compressed into smaller radii.

In order to show the dominance of DM over NM, in Fig. 7 we display the total mass (top panel) and only

P_{DM}/P_{NM}	M_T (M_\odot)	M_{NM} (M_\odot)	M_{DM} (M_\odot)	R_{NM} (km)	R_{DM} (km)	P_{NM} (MeV/fm ³)
10^{-1}	2.36	2.05	0.31	11.9	22.8	362
10^{-1}	2.12	1.19	0.93	12.9	60.0	33
10^{-1}	2.90	0.11	2.78	20.0	109.7	1
10^1	6.95	6.36×10^{-2}	6.88	3.2	53.0	997
10^1	6.68	0.10	6.58	4.60	49.78	199
10^1	7.98	2.59×10^{-2}	7.96	20.0	97.8	8×10^{-2}
10^3	7.16	1.72×10^{-4}	7.16	0.60	53.0	75.0
10^3	6.54	2.53×10^{-4}	6.54	1.24	49.3	2
10^3	7.60	9.12×10^{-4}	7.60	20.0	99.9	6×10^{-4}

TABLE V. Masses and radii of the normal matter and dark matter components for some of the stable objects obtained for $P_{DM}/P_{NM} = 10^{-1}, 10^1$ and 10^3 with $y = 10^3$ and $m_D = 5$ GeV. We also show the value of the central pressure for normal matter.

the DM contribution to the total mass (bottom panel) as a function of the DM radius for the same P_{DM}/P_{NM} shown in the bottom right plot of Fig. 3. We consider DM admixed stars with the normal matter radius

$R_{NM} < 20$ km. First, we observe that the DM radius is always much larger than the observable one (R_{NM}). In Table V we show the features of some of the stable objects displayed in Fig. 7.

As seen in Table V, all of these compact objects have a core formed by a mixture of NM and DM, surrounded by a DM halo. The structure of these objects is completely different to what we obtained for the other DM parametrizations explored in the previous sections ($m_D = 100$ GeV as well as $m_D = 5$ GeV for the weakly interacting case), where the DM radius was always much smaller than the NM one, so that the DM accumulated only in the core of the stars. Actually, these mass-radius configurations for low m_D and strongly interacting DM were reported in Refs. [25, 45, 71], but here we find an even more extreme scenario, with the DM radius exceeding more than four times the size of the core in all cases but one. Because these configurations resemble oysters, with the DM halo representing a large black shell and the NM core the small bright shining pearl (even though there is also DM mixed in this core), we have named these objects dark oysters.

As DM is dominating and increasing the mass of the stars, one would expect that the critical mass would also augment. And, in fact, that is what we observe when we plot the critical mass M_{crit} as a function of P_{DM}/P_{NM} . As can be seen in Fig. 8, the behavior of the critical mass is very different from what we have seen in the previous sections. For low P_{DM}/P_{NM} , M_{crit} is decreasing with the increase of the P_{DM}/P_{NM} . However, at $P_{DM}/P_{NM} = 8 \times 10^{-2}$ the behavior completely changes and M_{crit} quickly increases.

Apart from the different behavior of the critical mass with the P_{DM}/P_{NM} ratio, we find that some values of M_{crit} correspond to unstable stars. In Fig. 8 the dashed lines represent these unstable solutions, where the star with $P_{NM} = 361$ MeV/fm³, which is the pres-

sure where the hadron-quark phase transition happens, is unstable. However, as the NM central pressure is increased, for the same P_{DM}/P_{NM} , we get stable stars again, which, of course, are hybrid. This would be the case of $P_{DM}/P_{NM} = 10^1$ or $P_{DM}/P_{NM} = 10^3$ if M_{crit} were located somewhere between $50 < R_{DM} < 70$ km in Fig. 7 or $5 < R_{NM} < 9$ km in the bottom right of Fig. 3. The solid lines represent stable solutions and the dots correspond to the critical masses shown in Fig. 7. Note that the critical mass for $P_{DM}/P_{NM} = 10^3$ falls into a gap in the $M_{\text{crit}} \times P_{DM}/P_{NM}$ line. This is because this M_{crit} corresponds to unstable star configurations and, differently to the results that fall on the dashed lines, here, with the increase of the central pressure no stable hybrid star ever appears in our calculations.

At this point we should mention that, although the stability analysis used here is a step forward from the naive analysis done in previous works as we consider here the changes that the NM may induce on the DM and vice versa, it is not totally clear that, at high pressures, the change in stability showed by our stability analysis really corresponds to the change of the lowest energy mode ω_0 . So, our results for large pressures should be regarded with a grain of salt. A rigorous stability analysis of two-fluid stars is left to future work.

Regarding the quantity of QM, it can be larger than any of the cases analyzed in the previous section, which might be counterintuitive, considering that DM is strongly dominating over the NM. As we can see from Fig. 7, for $P_{DM}/P_{NM} = 10$ the contribution to the total mass coming from the NM seems negligible. In fact, for the star with $M_T = 6.95M_\odot$, NM only contributes with $6.36 \times 10^{-2}M_\odot$. However, for the same star, QM accounts

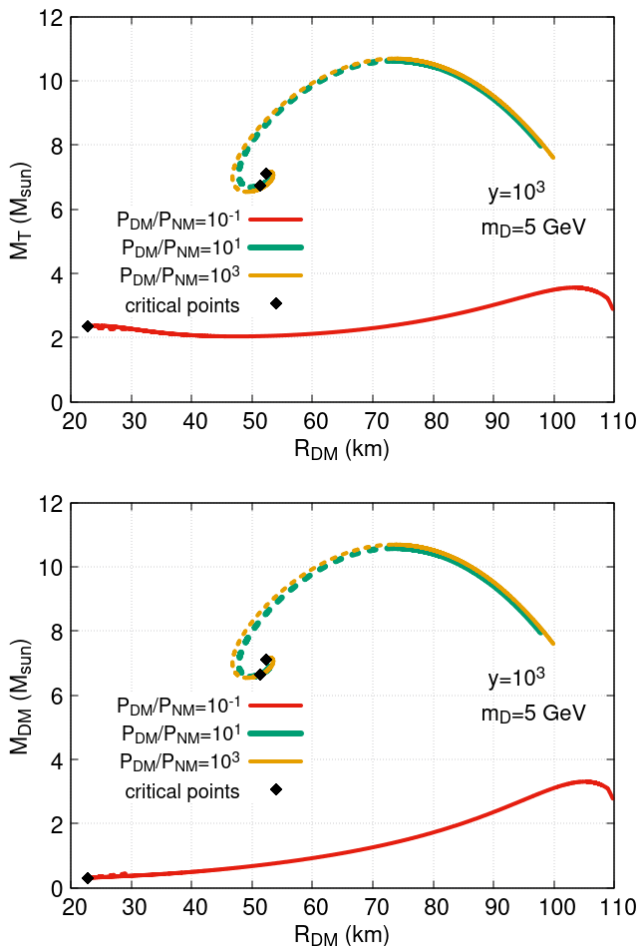


FIG. 7. Total mass (top panel) and DM mass (bottom panel) as a function of the DM radius for strongly interacting DM ($y = 10^3$) and $m_D = 5$ GeV for different pressure ratios for values of the observable radius $R_{NM} < 20$ km. The dots indicate the critical mass M_{crit} at which hybrid stars start to appear for each configuration. We also include the unstable results (dashed lines). Note that M_{crit} for $P_{DM}/P_{NM} = 10^3$ is actually also unstable.

for $2.01 \times 10^{-2} M_{\odot}$, which is more than we did obtain in the previous cases (see Fig. 6). Of course, the relative contribution of QM to the total mass is much less than in the previous cases.

Before finalizing this section, we should make some comments about the dominance of DM. We have analyzed stars with $R < 20$ km for $y = 10^3$ with $m_D = 5$ GeV, where DM dominates. In this case, the effect of DM is to increase the total mass of the stars, and, at the same time to decrease the observable radius. For the other combinations of y and m_D explored in the previous section, we have concentrated on the NS branch and DM that is not the dominant component. In that context, the effect of the DM is to first 'eat' away the NS branch, making the results migrate to the white dwarf branch, i.e., to larger radii (larger than 20 km) and then, eventually, to

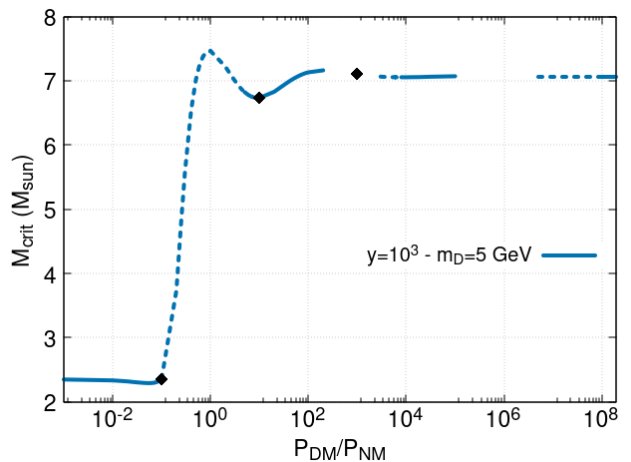


FIG. 8. Critical mass M_{crit} as a function of the DM pressure ratios P_{DM}/P_{NM} for strongly interacting DM $y = 10^3$ and particle mass $m_D = 5$ GeV. The solid lines represent stable stars. As for the dashed lines, the first hybrid star is unstable, but, at higher central pressures, maintaining the same ratio P_{DM}/P_{NM} , stable ones appear. The dots correspond to the critical masses for the three cases shown in Fig. 7.

smaller masses and radii to form the DCPs. This means that, if we keep on increasing the pressure ratios for that cases so that the DM becomes dominant, eventually we would obtain very small M_{crit} associated to objects with very small radii, that is, we would observe hybrid dark compact planets. The exploration of such results is kept for future works.

As already mentioned above, the increase in the total mass of DM admixed stars at low m_D was already reported in [25, 45, 71], although the discussion on the DM halo was scarce. In fact, those works show that the dark oyster configurations are also possible for weakly interacting DM as long as the particle mass is decreased even further. No work, however, to the best of our knowledge, has ever reported on dark oysters with a hybrid core.

VI. CONCLUSIONS

In this paper, we have investigated the effect of DM on hybrid stars using a two-fluid approach, considering that NM and DM interact only gravitationally. For NM we have built an EoS for hybrid stars via the Maxwell construction from a QHD-based model, for nucleons and hyperons, and a MIT-based model for uds-quark matter. For the DM EoS we use a non-selfannihilating self-interacting Fermi gas with different interaction strengths and two different particle masses, $m_D = 5$ GeV and $m_D = 100$ GeV.

We have found that the presence of DM in NSs may trigger the appearance of QM in its core at unprecedented low masses, giving rise to DM-admixed hybrid stars. This happens because the presence of DM causes an increase

of the central pressure of the NS, which, after a certain amount of DM is added, reaches the hadron-quark phase transition value. In a star that already has a QM core, the presence of DM will enhance this core. The amount of DM (in terms of the P_{DM}/P_{NM} ratio) that needs to be accumulated in order for the central pressure to increase depends on its interaction strength y and particle mass m_D : for weakly interacting DM one needs to add more DM than for the strongly interacting case and for the same interaction strength y , one needs to add more DM when the DM particle mass is larger. A direct consequence of this result is that the critical mass, i.e., the minimal mass of the star with a quark core, decreases with the increase of P_{DM}/P_{NM} . Except for strongly interacting DM with $m_D = 5$ GeV, we have shown that, by only analyzing the mass and the radius of the star, it is impossible to know the NM central pressure and if this central pressure allows the appearance of QM. The DM is then masquerading hybrid stars.

We have also determined that the quantity of each type of matter (hadron, quark and dark) that can accumulate in such stars depends on the interaction strength and DM particle mass, so that the DM parametrization that is more effective in compressing the star also gives rise to more QM, i.e., the changes in QM follow the ones for DM. Except for the strongly interacting DM with $m_D = 5$ GeV, we have obtained DM-admixed hybrid stars with very small QM cores and slightly larger DM cores.

In the last section we have carefully analyzed the results for a DM where $y = 10^3$ and $m_D = 5$ GeV. In this case we obtained what we named dark oysters, stars with a large DM radius and small observable radius of ordinary matter. Here, the addition of DM augments

the total mass of the star. Such results were already observed in Refs. [25, 45, 71], but to the best of our knowledge, the present work is the first to report on dark oysters with a hybrid core. In fact, for the dark oyster we have shown that QM mass can be larger than for the other DM parametrizations we have explored in this work. Dark oysters could be observable by measuring for example neutron stars with a seemingly unphysically small radii of just a few kilometres while having a large total gravitational masses of several solar masses.

ACKNOWLEDGEMENTS

C.B. received support from the Conselho Nacional de Desenvolvimento Científico e Tecnológico (CNPq/Brazil) and thanks the Institute of Space Sciences (ICE, CSIC) for hosting her during a year. L.T. acknowledges support from CEX2020-001058-M (Unidad de Excelencia “María de Maeztu”) and PID2022-139427NB-I00 financed by the Spanish MCIN/AEI/10.13039/501100011033/FEDER,UE as well as from the Generalitat de Catalunya under contract 2021 SGR 171 and from the Generalitat Valenciana under contract CIPROM/2023/59. L.T. and J.S.B. acknowledge support by the CRC-TR 211 ‘Strong-interaction matter under extreme conditions’- project Nr. 315477589 - TRR 211.

REFERENCES

-
- [1] G. Bertone, D. Hooper, and J. Silk, *Physics Reports* **405**, 279–390 (2005).
 - [2] A. et al. (Planck Collaboration), *A & A* **641**, A6 (2020).
 - [3] M. B. et al. (SDSS Collaboration), *A&A* **568**, A22 (2014).
 - [4] P. A. Ade, N. Aghanim, M. Arnaud, M. Ashdown, J. Aumont, C. Baccigalupi, A. Banday, R. Barreiro, J. Bartlett, N. Bartolo, *et al.*, *Astronomy & Astrophysics* **594**, A13 (2016).
 - [5] A. G. and A. T. et al. (ATLAS Collaboration), *Journal of High Energy Physics* **75** (2013), 10.1007/JHEP04(2013)075.
 - [6] C. S. and K. V. et al. (CMS Collaboration), *Journal of High Energy Physics* **94** (2012), 10.1007/JHEP09(2012)094.
 - [7] M. Klasen, M. Pohl, and G. Sigl, *Progress in Particle and Nuclear Physics* **85**, 1 (2015).
 - [8] I. Goldman and S. Nussinov, *Phys. Rev. D* **40**, 3221 (1989).
 - [9] L. Brayeur and P. Tinyakov, *Phys. Rev. Lett.* **109**, 061301 (2012).
 - [10] C. Kouvaris, *Physical Review D* **77** (2008), 10.1103/physrevd.77.023006.
 - [11] C. Kouvaris and P. Tinyakov, *Phys. Rev. Lett.* **107**, 091301 (2011).
 - [12] J. Fuller and C. D. Ott, *Monthly Notices of the Royal Astronomical Society: Letters* **450**, L71 (2015).
 - [13] J. F. Acevedo, J. Bramante, A. Goodman, J. Kopp, and T. Opferkuch, *Journal of Cosmology and Astroparticle Physics* **2021**, 026 (2021).
 - [14] A. Ray, *Phys. Rev. D* **107**, 083012 (2023).
 - [15] S. Bhattacharya, B. Dasgupta, R. Laha, and A. Ray, *Phys. Rev. Lett.* **131**, 091401 (2023).
 - [16] S. Bhattacharya, A. L. Miller, and A. Ray, *Physical Review D* **110** (2024), 10.1103/physrevd.110.043006.
 - [17] C. Kouvaris and P. Tinyakov, *Phys. Rev. D* **83**, 083512 (2011).
 - [18] G. Bertone and M. Fairbairn, *Phys. Rev. D* **77**, 043515 (2008).
 - [19] C. Kouvaris and P. Tinyakov, *Phys. Rev. D* **82**, 063531 (2010).
 - [20] M. McCullough and M. Fairbairn, *Phys. Rev. D* **81**, 083520 (2010).

- [21] A. de Lavallaz and M. Fairbairn, *Phys. Rev. D* **81**, 123521 (2010).
- [22] A. Sedrakian, *Phys. Rev. D* **99**, 043011 (2019).
- [23] S. A. Bhat and A. Paul, *The European Physical Journal C* **80** (2020), 10.1140/epjc/s10052-020-8072-x.
- [24] M. Ángeles Pérez-García and J. Silk, *Physics Letters B* **711**, 6 (2012).
- [25] M. Deliyergiyev, A. Del Popolo, L. Tolos, M. Le Delliou, X. Lee, and F. Burgio, *Phys. Rev. D* **99**, 063015 (2019).
- [26] S. Blinnikov and M. Y. Khlopov, *Soviet Astronomy*, vol. 27, July-Aug. 1983, p. 371-375. Translation *Astronomicheskii Zhurnal*, vol. 60, July-Aug. 1983, p. 632-639 **27**, 371 (1983).
- [27] M. Khlopov, G. Beskin, N. Bochkarev, L. Pustilnik, and S. Pustilnik, *Observational physics of mirror world*, Tech. Rep. (1989).
- [28] A. Li, F. Huang, and R.-X. Xu, *Astroparticle Physics* **37**, 70 (2012).
- [29] F. Sandin and P. Ciarcelluti, *Astroparticle Physics* **32**, 278 (2009).
- [30] S.-C. Leung, M.-C. Chu, and L.-M. Lin, *Phys. Rev. D* **84**, 107301 (2011).
- [31] S.-C. Leung, M.-C. Chu, and L.-M. Lin, *Phys. Rev. D* **85**, 103528 (2012).
- [32] Q.-F. Xiang, W.-Z. Jiang, D.-R. Zhang, and R.-Y. Yang, *Phys. Rev. C* **89**, 025803 (2014).
- [33] I. Goldman, R. Mohapatra, S. Nussinov, D. Rosenbaum, and V. Teplitz, *Physics Letters B* **725**, 200–207 (2013).
- [34] M. Khlopov, *International Journal of Modern Physics A* **28**, 1330042 (2013).
- [35] P. Mukhopadhyay and J. Schaffner-Bielich, *Phys. Rev. D* **93**, 083009 (2016).
- [36] L. Tolos and J. Schaffner-Bielich, *Phys. Rev. D* **92**, 123002 (2015).
- [37] Y. Dengler, J. Schaffner-Bielich, and L. Tolos, *Phys. Rev. D* **103**, 109901 (2021).
- [38] Z. Rezaei, *The Astrophysical Journal* **835**, 33 (2017).
- [39] G. Panotopoulos and I. Lopes, *Phys. Rev. D* **96**, 083004 (2017).
- [40] A. E. Nelson, S. Reddy, and D. Zhou, *Journal of Cosmology and Astroparticle Physics* **2019**, 012 (2019).
- [41] J. Ellis, G. Hütsi, K. Kannike, L. Marzola, M. Raidal, and V. Vaskonen, *Phys. Rev. D* **97**, 123007 (2018).
- [42] M. I. Gresham and K. M. Zurek, *Phys. Rev. D* **99**, 083008 (2019).
- [43] A. Del Popolo, M. Deliyergiyev, M. Le Delliou, L. Tolos, and F. Burgio, *Physics of the Dark Universe* **28**, 100484 (2020).
- [44] O. Ivanytskyi, V. Sagun, and I. Lopes, *Phys. Rev. D* **102**, 063028 (2020).
- [45] Y. Dengler, J. Schaffner-Bielich, and L. Tolos, *Phys. Rev. D* **105**, 043013 (2022).
- [46] D. Rafei Karkevandi, S. Shakeri, V. Sagun, and O. Ivanytskyi, *Phys. Rev. D* **105**, 023001 (2022).
- [47] D. Sen and A. Guha, *Monthly Notices of the Royal Astronomical Society* **504**, 3354 (2021).
- [48] A. Guha and D. Sen, *Journal of Cosmology and Astroparticle Physics* **2021**, 027 (2021).
- [49] Z. Miao, Y. Zhu, A. Li, and F. Huang, *The Astrophysical Journal* **936**, 69 (2022).
- [50] D. Sen and A. Guha, *Monthly Notices of the Royal Astronomical Society* **517**, 518 (2022).
- [51] O. Ferreira and E. S. Fraga, *Journal of Cosmology and Astroparticle Physics* **2023**, 012 (2023).
- [52] S. Shakeri and D. R. Karkevandi, *Phys. Rev. D* **109**, 043029 (2024).
- [53] M. Hippert, E. Dillingham, H. Tan, D. Curtin, J. Noronha-Hostler, and N. Yunes, *Physical Review D* **107** (2023), 10.1103/physrevd.107.115028.
- [54] M. Cassing, A. Brisebois, M. Azeem, and J. Schaffner-Bielich, *The Astrophysical Journal* **944**, 130 (2023).
- [55] R. Zöllner and B. Kämpfer, *Astronomy* **1**, 36 (2022).
- [56] M. Collier, D. Croon, and R. K. Leane, *Phys. Rev. D* **106**, 123027 (2022).
- [57] C. H. Lenzi, M. Dutra, O. Lourenço, L. L. Lopes, and D. P. Menezes, *The European Physical Journal C* **83**, 1 (2023).
- [58] R. Zöllner, M. Ding, and B. Kämpfer, *Particles* **6**, 217 (2023).
- [59] J. Cronin, X. Zhang, and B. Kain, *Phys. Rev. D* **108**, 103016 (2023).
- [60] P. Thakur, T. Malik, A. Das, T. K. Jha, and C. m. c. Providência, *Phys. Rev. D* **109**, 043030 (2024).
- [61] V. Sagun, E. Giangrandi, T. Dietrich, O. Ivanytskyi, R. Negreiros, and C. Providência, *The Astrophysical Journal* **958**, 49 (2023).
- [62] M. Mariani, C. Albertus, M. d. R. Alessandroni, M. G. Orsaria, M. Á. Pérez-García, and I. F. Ranea-Sandoval, *Monthly Notices of the Royal Astronomical Society* **527**, 6795 (2024).
- [63] R. F. Diedrichs, N. Becker, C. Jockel, J.-E. Christian, L. Sagunski, and J. Schaffner-Bielich, *Phys. Rev. D* **108**, 064009 (2023).
- [64] H.-M. Liu, J.-B. Wei, Z.-H. Li, G. Burgio, and H.-J. Schulze, *Physics of the Dark Universe* **42**, 101338 (2023).
- [65] J. Bramante and N. Raj, *Physics Reports* **1052**, 1 (2024), dark matter in compact stars.
- [66] E. Giangrandi, A. Ávila, V. Sagun, O. Ivanytskyi, and C. Providência, *Particles* **7**, 179 (2024).
- [67] A. Guha and D. Sen, *Phys. Rev. D* **109**, 043038 (2024).
- [68] D. Rafei Karkevandi, M. Shahrabaf, S. Shakeri, and S. Typel, *Particles* **7**, 201 (2024).
- [69] H.-M. Liu, J.-B. Wei, Z.-H. Li, G. F. Burgio, H. C. Das, and H. J. Schulze, “Dark matter effects on the properties of neutron stars: compactness and tidal deformability,” (2024), arXiv:2403.17024 [nucl-th].
- [70] P. Ciarcelluti and F. Sandin, *Physics Letters B* **695**, 19 (2011).
- [71] M. F. Barbat, J. Schaffner-Bielich, and L. Tolos, *Phys. Rev. D* **110**, 023013 (2024).
- [72] S. L. Pitz and J. Schaffner-Bielich, (2024), arXiv:2408.13157 [astro-ph.HE].
- [73] S. Shirke, S. Ghosh, D. Chatterjee, L. Sagunski, and J. Schaffner-Bielich, *JCAP* **12**, 008 (2023), arXiv:2305.05664 [astro-ph.HE].
- [74] S. Shirke, B. K. Pradhan, D. Chatterjee, L. Sagunski, and J. Schaffner-Bielich, *Phys. Rev. D* **110**, 063025 (2024), arXiv:2403.18740 [gr-qc].
- [75] S. Pal and G. Chaudhuri, *Journal of Cosmology and Astroparticle Physics* **2024**, 064 (2024).
- [76] D. Ivanenko and D. Kurdgelaidze, *HYPOTHESIS CONCERNING QUARK STARS.*, Tech. Rep. (Moscow State Univ., 1965).

- [77] D. P. Menezes, *Universe* **7** (2021), 10.3390/universe7080267.
- [78] E. Annala, T. Gorda, A. Kurkela, J. Nättilä, and A. Vuorinen, *Nature Physics* **16**, 907 (2020).
- [79] A. Bodmer, *Physical Review D* **4**, 1601 (1971).
- [80] E. Witten, *Physical Review D* **30**, 272 (1984).
- [81] B. Lukács, J. Zimányi, and N. Balazs, *Physics Letters B* **183**, 27 (1987).
- [82] N. K. Glendenning, *Physical Review D* **46**, 1274 (1992).
- [83] L. L. Lopes, C. Biesdorf, and D. P. Menezes, *Monthly Notices of the Royal Astronomical Society* **512**, 5110 (2022).
- [84] G. Narain, J. Schaffner-Bielich, and I. N. Mishustin, *Phys. Rev. D* **74**, 063003 (2006).
- [85] B. Serot and J. Walecka, “Advances in nuclear physics, edited by jw negele and e. vogt,” (1986).
- [86] J. Boguta and A. Bodmer, *Nuclear Physics A* **292**, 413 (1977).
- [87] J. Boguta and H. Stoecker, *Phys. Lett. B* **120**, 289 (1983).
- [88] C. J. Horowitz and J. Piekarewicz, *Phys. Rev. Lett.* **86**, 5647 (2001), arXiv:astro-ph/0010227.
- [89] C. J. Horowitz and J. Piekarewicz, *Phys. Rev. C* **64**, 062802 (2001), arXiv:nucl-th/0108036.
- [90] G. Lalazissis, S. Karatzikos, R. Fossion, D. P. Arteaga, A. Afanasjev, and P. Ring, *Physics Letters B* **671**, 36 (2009).
- [91] L. L. Lopes and D. P. Menezes, *The Astrophysical Journal* **936**, 41 (2022).
- [92] M. Dutra, O. Lourenço, S. S. Avancini, B. V. Carlson, A. Delfino, D. P. Menezes, C. Providência, S. Typel, and J. R. Stone, *Phys. Rev. C* **90**, 055203 (2014).
- [93] M. Oertel, M. Hempel, T. Klähn, and S. Typel, *Rev. Mod. Phys.* **89**, 015007 (2017).
- [94] C. Biesdorf, D. P. Menezes, and L. L. Lopes, *Brazilian Journal of Physics* **53**, 137 (2023), 10.1007/s13538-023-01348-z.
- [95] C. Dover and A. Gal, *Progress in Particle and Nuclear Physics* **12**, 171 (1984).
- [96] J. Schaffner and I. N. Mishustin, *Phys. Rev. C* **53**, 1416 (1996).
- [97] S. Banik, M. Hempel, and D. Bandyopadhyay, *The Astrophysical Journal Supplement Series* **214**, 22 (2014).
- [98] L. Tolos, M. Centelles, and A. Ramos, *Publications of the Astronomical Society of Australia* **34**, e065 (2017).
- [99] L. Tolos, M. Centelles, and A. Ramos, *Astrophys. J.* **834**, 3 (2017), arXiv:1610.00919 [astro-ph.HE].
- [100] L. L. Lopes and D. P. Menezes, *Phys. Rev. C* **89**, 025805 (2014).
- [101] L. L. Lopes, C. Biesdorf, and D. P. Menezes, *Physica Scripta* **96**, 065303 (2021).
- [102] Particle Data Group, M. Tanabashi, K. Hagiwara, K. Hikasa, K. Nakamura, and Y. Nir, *Physical Review D* **98** (2018), 10.1103/PhysRevD.98.030001.
- [103] J. Negele and D. Vautherin, *Nuclear Physics A* **207**, 298 (1973).
- [104] S. B. Rüster, M. Hempel, and J. Schaffner-Bielich, *Phys. Rev. C* **73**, 035804 (2006).
- [105] B. K. Harrison, K. S. Thorne, M. Wakano, and J. A. Wheeler, *Gravitation theory and gravitational collapse* (1965).
- [106] O. Komoltsev and A. Kurkela, *Physical Review Letters* **128** (2022), 10.1103/physrevlett.128.202701.
- [107] K. Fukushima and T. Hatsuda, *Reports on Progress in Physics* **74**, 014001 (2010).
- [108] A. V. Olinto, *Physics Letters B* **192**, 71 (1987).
- [109] T. E. R. et. al., *The Astrophysical Journal Letters* **918**, L27 (2021).
- [110] R. W. Romani, D. Kandel, A. V. Filippenko, T. G. Brink, and W. Zheng, *The Astrophysical Journal Letters* **934**, L17 (2022).
- [111] J. Schaffner-Bielich, *Compact star physics* (Cambridge University Press, 2020).
- [112] A. Henriques, A. R. Liddle, and R. Moorhouse, *Physics Letters B* **251**, 511 (1990).
- [113] B. Kain, *Physical Review D* **103** (2021), 10.1103/physrevd.103.043009.
- [114] F. Di Giovanni, D. Guerra, S. Albanesi, M. Miravet-Tenés, and D. Tseneklidou, *Phys. Rev. D* **106**, 084013 (2022).
- [115] S. Valdez-Alvarado, C. Palenzuela, D. Alic, and L. A. Ureña-López, *Physical Review D* **87** (2013), 10.1103/physrevd.87.084040.
- [116] J. E. Nyhan and B. Kain, *Phys. Rev. D* **105**, 123016 (2022).
- [117] S. Weinberg, *Gravitation and Cosmology: Principles and Applications of the General Theory of Relativity* (Wiley, New York, 1972).